TO THE EDITOR:

Dual PD1/LAG3 immune checkpoint blockade limits tumor development in a murine model of chronic lymphocytic leukemia

Marina Wierz,[1] Sandrine Pierson,[1] Léa Guyonnet,[2,3] Elodie Viry,[1] Audrey Lequeux,[1] Anaïs Oudin,[4] Simone P. Niclou,[4] Markus Ollert,[2,5] Guy Berchem,[1,6] Bassam Janji,[1] Coralie Guérin,[2,3] Jerome Paggetti,[1,]* and Etienne Moussay[1,]*

[1]Laboratory of Experimental Cancer Research, Department of Oncology, [2]Department of Infection and Immunity, [3]National Cytometry Platform, Department of Infection and Immunity, and [4]NorLux Neuro-Oncology Laboratory, Department of Oncology, Luxembourg Institute of Health, Luxembourg, Luxembourg; [5]Department of Dermatology and Allergy Center, Odense Research Center for Anaphylaxis, University of Southern Denmark, Odense, Denmark; and [6]Centre Hospitalier de Luxembourg, Luxembourg, Luxembourg

Tissue-infiltrating chronic lymphocytic leukemia (CLL) cells come in direct contact with both accessory stromal and immune cells that compose the tumor microenvironment (TME). The proliferation and survival of CLL cells is highly dependent on complex interactions with nonmalignant cells of the TME.[1] Malignant cells are capable of suppressing antitumor immune responses by several mechanisms to escape immune surveillance,[2-4] including the dysregulation of immune checkpoints, which are surface proteins that regulate immune cell activation.[5,6] It has been demonstrated that CLL cells overexpress programmed cell death ligand 1 (PD-L1), resulting in increased PD-L1/PD1 signaling and, consequently, CD8^{+} T-cell functional silencing.[7,8] Immunotherapy aims to stimulate antitumor activity by reactivating the immune system and showed encouraging results in preclinical CLL studies.[9] Here, we established an extensive cartography of immune cell subsets populating the leukemic microenvironment in a murine model of CLL, as well as their immune checkpoint profile, and evaluated the efficacy of a relevant dual immunotherapy in a preclinical study.

We performed adoptive transfer (AT) of splenocytes from diseased Eμ-TCL1 mice into C57BL/6 recipient mice. Mice were killed when CD5^{+}CD19^{+} CLL cells represented 75% of peripheral blood mononuclear cells (PBMCs) (~5 weeks). Single-cell suspensions were prepared from spleens and analyzed by mass cytometry (n = 6) with a custom 35-marker panel (supplemental Table 1, available on the *Blood* Web site) to identify and characterize immune cells from the TME. Besides the enrichment in CLL cells in AT-TCL1 (mean, 84.3%; range, 77.9 to 87.2%) (Figure 1A; supplemental Figure 1A), we observed that compared with normal B cells, CLL cells showed a higher expression for cell adhesion molecules, immune checkpoints, and intracellular cytokines (Figure 1B). PD-L1 is heterogeneously expressed on splenic CLL cells. A high expression is associated with high expression of maturation/adhesion molecules. Moreover, blood cells showed a lower expression for all these molecules than splenic cells (supplemental Figure 1B), suggesting the presence of different stages of recirculating cells in the spleen.[8] Next, B cells were excluded from our analysis to focus on other immune cells (CD45^{+}CD19^{−}B220^{−}). We observed that CD4^{+} T cells are decreased in diseased animals

while regulatory T (Treg) cells, monocytes, macrophages, dendritic cells, and mesenchymal stem cells/cancer-associated fibroblasts are more abundant (supplemental Figure 2A-B). The viSNE algorithm was used to generate immune maps of the spleen (Cytobank, Figure 1C; supplemental Figure 2C). Then, the SPADE unsupervised algorithm generated 50 clusters of immune cells (supplemental Figure 2D) that were overlaid on viSNE plots to visualize immune subpopulations. Fifteen clusters were enriched in AT-TCL1 mice (*P* < .01), while 18 clusters were decreased and 17 remained unchanged (Figure 1D; supplemental Figure 2E). Immune cell clusters enriched compared with C57BL/6 and of specific interest were further characterized. Although the overall frequency of CD8^{+} T cells was not affected, some specific subpopulations were enriched in AT-TCL1 mice, whereas others were reduced (Figure 1E; supplemental Figure 2F). Indeed, we noted a significant increase in effector memory (cluster 50) and central memory (cluster 14) cells along with 2 large clusters of activated CD38^{+}CD69^{+} effector cells displaying features of exhaustion, such as high expression of PD1, LAG3, TIM3, and CTLA4 (clusters 31 and 17). Interestingly, three clusters of Treg cells were identified (Figure 1F). Cells from cluster 46/C represent terminally differentiated KLRG1^{+}CD69^{+} Treg cells described as tumor-infiltrating Treg cells.[10,11] In addition, the higher abundance of Foxp3^{+}CD25^{low}LAG3^{+} Treg cells (cluster 10/B) also reveals the recruitment of a reservoir of committed CD25^{low} Treg cells shown to efficiently suppress humoral immune response.[12,13] These 2 clusters are enriched in AT-TCL1 mice and express high levels of PD1, LAG3, KLRG1, and CTLA4. Such phenotype reflects cells with enhanced suppressive capacities.[14,15] In contrast, the density of naive CD44^{low}CD62L^{+}CD38^{−}PD1^{−}KLRG1^{−} Treg cells (cluster 41/A) was not altered in AT-TCL1 mice. Therefore, fully activated Treg cells became the majority, suggesting an immunosuppressive microenvironment (increased B/A and C/A ratios). Concerning myeloid cells, CD8^{+} dendritic cells (cDCs; cluster 49) were augmented in CLL mice (Figure 1G). These highly suppressive cDCs usually fail to induce an effective CD4^{+} T cell response[16] and have the capacity to induce Foxp3^{+} Treg cells.[17] Moreover, we confirmed the induction of CLL-promoting patrolling monocytes in AT-TCL1 mice recently described (Figure 1H).[9,18] More specifically, although all subsets of monocytes were more
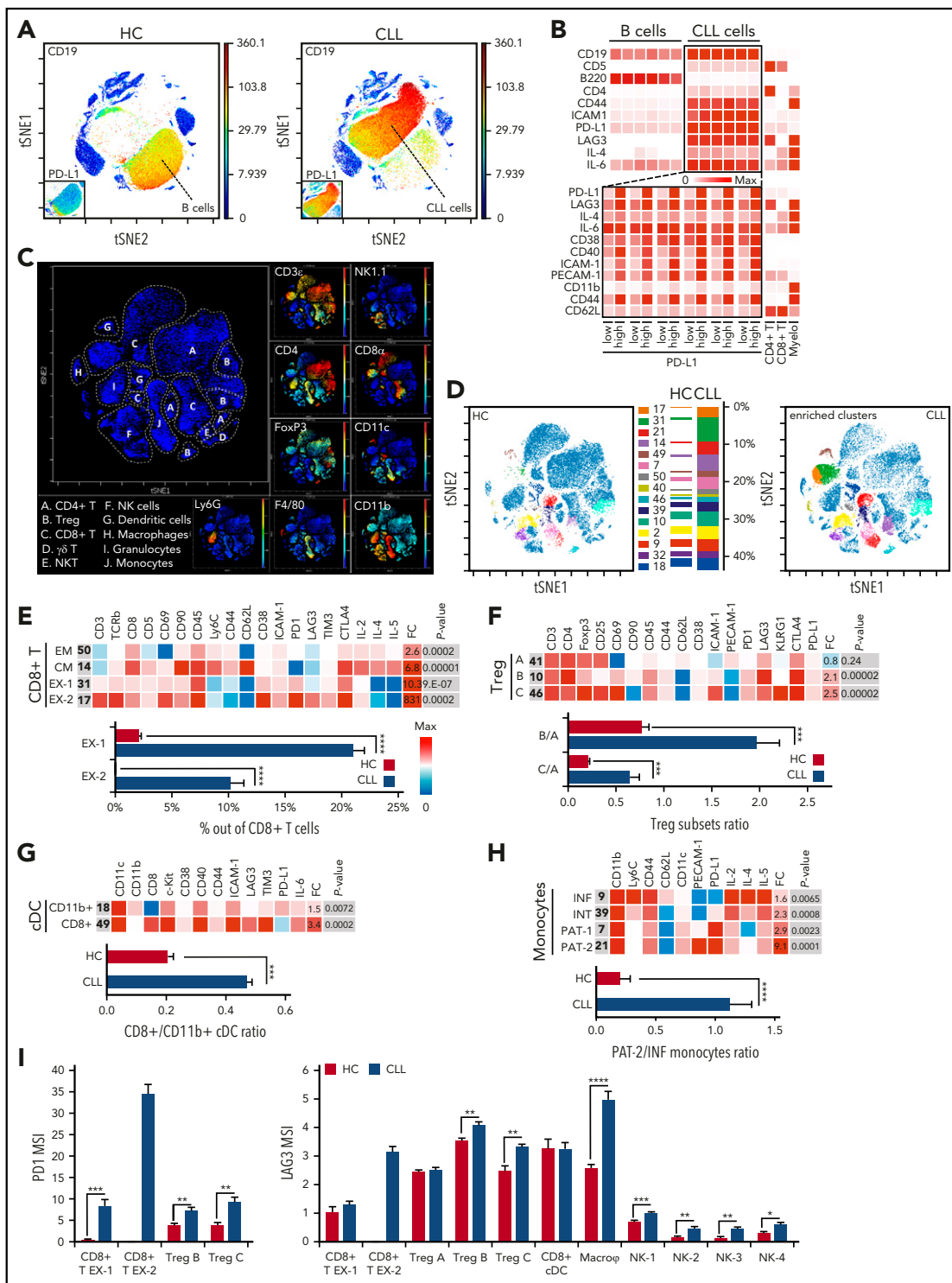
Figure 1. High-dimensional mass cytometry analysis of murine splenocytes. (A) viSNE plots (Cytobank) allowing the visualization of CD45+ splenocytes from healthy controls (HC) C57BL/6 (left) and AT-TCL1 (right, CLL) mice on 2 dimensions based on the expression of all markers. The main plot depicts CD19 expression. The lower left box displays PD-L1 expression on B and CLL cells, respectively. Blue indicates the absence of expression; red indicates the highest expression among all cells and all samples. (B) Heatmap plotting the median signal intensity of discriminative markers between normal B and CLL cells (top panel, n = 6). Heatmap plotting the median expression of markers between PD-L1low (MSI<20) and PD-L1high (MSI>90) CLL cells (bottom panel, n = 6). Expression in CD4+ T cells, CD8+ T cells, and CD11b+ myeloid cells from C57BL/6 mice was plotted as references. (C) viSNE plots illustrating splenic live CD45+CD19−B220− immune cell populations from AT-TCL1 mice (left) and characteristic marker expression (right). (D) The 15 enriched clusters (P < .01) in AT-TCL1 mice (CLL) compared with C57BL/6 were overlaid on the viSNE plots. The color scale depicts the cluster number and the related percentage of cells within live CD45+CD19−B220− cells. (E-H) Heatmaps plotting the median signal intensity of discriminative markers between different clusters of immune cells in AT-TCL1 mice. Selected clusters show a significant enrichment of CD8+ T cells (E), Treg cells (F), cDCs (G), and monocytes (H) in AT-TCL1 compared with C57BL/6 mice (fold change [FC], P value). Bar charts represent percentages of cells or ratios observed between C57BL/6 (HC, n = 6) and AT-TCL1 (CLL, n = 6) mice. CM central memory; EM, effector memory; EX exhausted; INF inflammatory; INT intermediate. (I) Mean signal intensity (MSI) of PD1 and LAG3 expression on relevant immune cell subpopulations. NK, natural killer. For all panels, *P < .05, **P < .01, ***P < .001, and ****P < .0001.
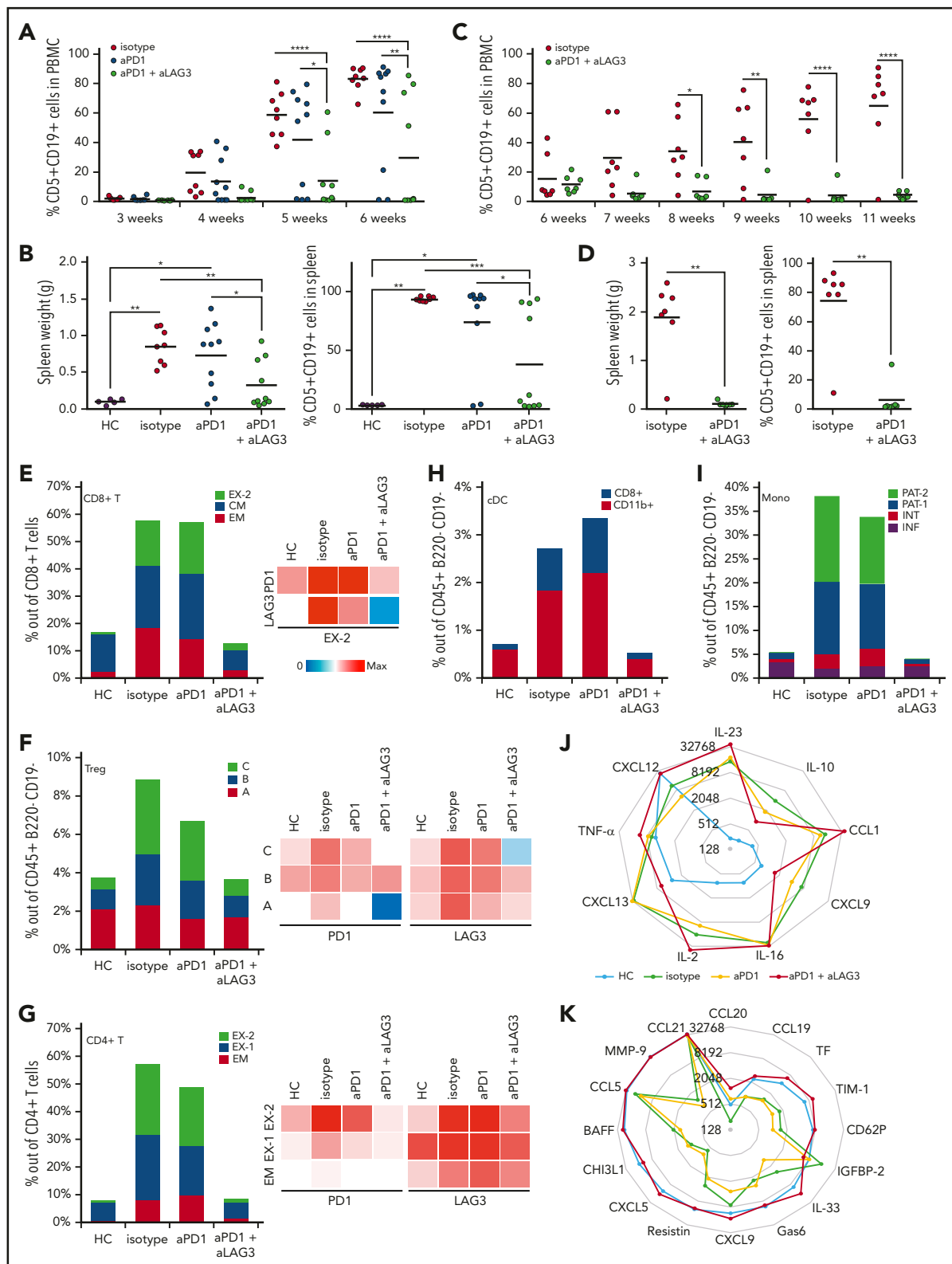
Figure 2. Dual PD1 and LAG3 blockade limits CLL development and restores immune cell populations. (A-D) The tumor load of individual mice is depicted by the percentage of CD5⁺CD19⁺ cells in the peripheral blood (A,C) and spleen (B,D; weight in grams [left] and percentage of CD5⁺CD19⁺ [right]) in 2 independent cohorts (cohort 1, A-B and cohort 2, C-D). For all panels, *P < .05, **P < .01, ***P < .001, ****P < .0001. (E-I) Bar charts representing the percentage of cells present in healthy controls C57BL/6 (HC, n = 3) and AT-TCL1 mice following therapy (isotype, aPD1, or aPD1 + aLAG3, n = 3 from cohort 1). Selected clusters showing a significant enrichment are depicted for CD8⁺ T cells (E), Treg cells (F), CD4⁺ T cells (G), cDCs (H), and monocytes (I) in AT-TCL1 compared with C57BL/6 mice and a decrease upon dual aPD1 + aLAG3 therapy. Heatmaps represent the median signal intensity of PD1 and LAG3 in selected subsets of immune cells. CM central memory; EM effector memory; EX exhausted; INF, inflammatory; INT, intermediate. (J-K) Levels of selected cytokines and soluble factors in blood serum (J) and spleen plasma (K) from C57BL/6 (HC, n = 3) and AT-TCL1 mice following therapy (isotype, aPD1, or aPD1 + aLAG3, n = 3 from cohort 1, same animals as E-I), quantified using mouse cytokine arrays.

abundant, 2 subpopulations of Ly6C^{low}CD44$^+$PD-L1^{high} patrolling (PAT) monocytes, distinguished by their expression of PECAM-1 (CD31) and IL-4, were particularly enriched in AT-TCL1 mice. As CD31 ligation leads to inflammatory cytokines secretion,[19] PAT-2 monocytes exhibit an even stronger protumorigenic potential. Finally, we showed that PD1 and LAG3 expression was high/increased in most of these clusters (CD8$^+$ T cells, Treg cells, macrophages, and natural killer cells; Figure 1I), reflecting the exhausted (CD8$^+$ T cells) or activated (Treg cells) state of immune cells. Importantly, the results observed in AT-TCL1 mice were confirmed by mass cytometry in diseased Eμ-TCL1 mice (supplemental Figures 3 and 4). Although the proportion of some immune cell populations differed (slight increase in CD8$^+$ T cells and granulocytes, supplemental Figure 4C), the enrichment in specific immune cell subsets was very similar between AT-TCL1 and Eμ-TCL1 mice (supplemental Figure 4E-J). Altogether, CLL induces a dramatic remodeling of splenic immune cell populations, thus favoring an immunosuppressive microenvironment with altered antitumor immunity. Therefore, we hypothesized that an antibody-based therapy targeting multiple immune checkpoints could restore a functional antitumor immune response.

For this purpose, we designed a protocol to treat AT-TCL1 mice with single- or dual- antibody–based therapy. Single anti-PD1, single anti-LAG3, single anti-KLRG1, and dual anti-PD1/KLRG1 treatments resulted in slight or no improvement regarding CLL progression (supplemental Figure 5E-G). Importantly, dual anti-PD1/LAG3 therapy was the most efficient, as both the percentage and the number of CLL cells remained significantly lower in blood and spleen. Splenocytes from independent donors were transferred to 2 cohorts of recipient mice. Although the disease developed at different pace in both cohorts, dual blockade resulted in disease-free animals, showing regular spleen weight and absence of CLL cells (Figure 2A-D; supplemental Figure 5A-D).

Splenocytes from animals successfully treated (PD1/LAG3 therapy, cohort 1), along with C57BL/6 and diseased AT-TCL1 mice (isotype and anti-PD1 treated), were analyzed by mass cytometry with the same methodology (supplemental Figure 6A-D). Similar or higher alterations in immune cell compositions and phenotypes were observed in mice treated with isotype or anti-PD1 antibodies, reflecting a more advanced disease (95% CLL cells in spleen) than that seen in mice shown in Figure 1 (Figure 2E-I; supplemental Figure 6E-G). Dual therapy corrected the imbalance generated by CLL and restored an immunocompetent environment with fewer Treg cells and myeloid cells and more T cells. Phenotyping of the second cohort confirmed a switch from antigen-experienced/effector T cells to naive cells similarly to anti-PD-L1 therapy.[9] The percentage of PD1$^+$ and PD1$^+$LAG3$^+$ T cells also strikingly decreased after therapy (supplemental Figure 6H-K). Of great importance, dual therapy also significantly reduced spleen volume in diseased Eμ-TCL1 mice (supplemental Figure 7A-B). Notably, we identified strong correlations between the decrease in spleen volume and T-cell phenotypes in the peripheral blood before treatment (percentages of naive or antigen-experienced/effector CD4$^+$ and CD8$^+$ T cells, ratio of CD4$^+$/CD8$^+$ T cells) (supplemental Figure 7C-G). Altogether, these data demonstrate that dual PD-1/LAG3 blockade efficiently decreases tumor load in CLL-diseased animals.

Next, we quantified cytokines in blood serum and spleen plasma to better characterize the microenvironment. The disease greatly influenced the cytokine profiles in both compartments with an increase of specific cytokines in the serum (CXCL13, CXCL9, interleukin 10 [IL-10], and IL-16) and a decrease in the spleen (BAFF, MMP9, IL-33, and CXCL5) (Figure 2J-K; supplemental Figure 8), reflecting leukocyte chemoattraction from the periphery and a local immunosuppression within the TME. Animals successfully treated by dual therapy presented an altered cytokine profile in circulation compared with healthy controls. Dual blockade restored an immune response exemplified by increased levels of IL-2, IL-23, tumor necrosis factor α, and CCL1 in serum. Cytokine profiles of dual-treated nonresponsive animals significantly differed from responsive animals (supplemental Figure 8C,F) and resembled the ones of diseased animals (isotype or anti-PD1 treated).

In conclusion, we expanded the current knowledge regarding immune cell populations present in the CLL TME and demonstrated that dual targeting of immune checkpoints PD1 and LAG3 successfully controlled CLL development in preclinical mouse models and therefore could represent an effective treatment to restore a functional antitumor immune response.

Authorship

Contribution: J.P. and E.M. designed the study and analyzed data. M.W., S.P., E.V., A.L., A.O., J.P. performed animal experimentation, flow cytometry and analyzed data. L.G. and C.G. performed mass cytometry experiments and analyzed data. A.O. and S.P.N. performed MRI analysis. M.W., J.P., and E.M. prepared the figures and wrote the paper. M.O., G.B., B.J., J.P., and E.M. supervised the study. All authors revised the manuscript.

Conflict-of-interest disclosure: The authors declare no competing financial interests.

ORCID profiles: M.W., 0000-0002-4636-7671; J.P., 0000-0001-9460-5876; E.M., 0000-0002-0879-8067.

Correspondence: Jerome Paggetti, Laboratory of Experimental Cancer Research, Department of Oncology, Luxembourg Institute of Health, 84 Val Fleuri, L-1526, Luxembourg, Luxembourg; e-mail: jerome.paggetti@lih.lu; and Etienne Moussay, Laboratory of Experimental Cancer Research, Department of Oncology, Luxembourg Institute of Health, 84 Val Fleuri, L-1526, Luxembourg, Luxembourg; e-mail: etienne.moussay@lih.lu.

Footnotes

*J.P. and E.M. contributed equally to this study.

The online version of this article contains a data supplement.

REFERENCES

1. Burger JA, Ghia P, Rosenwald A, Caligaris-Cappio F. The microenvironment in mature B-cell malignancies: a target for new treatment strategies. *Blood.* 2009;114(16):3367-3375.

2. Goldman B, DeFrancesco L. The cancer vaccine roller coaster. *Nat Biotechnol.* 2009;27(2):129-139.

3. Cutucache CE. Tumor-induced host immunosuppression: special focus on CLL. *Int Immunopharmacol.* 2013;17(1):35-41.

4. Curran EK, Godfrey J, Kline J. Mechanisms of immune tolerance in leukemia and lymphoma. *Trends Immunol.* 2017;38(7):513-525.

5. Pardoll DM. The blockade of immune checkpoints in cancer immunotherapy. *Nat Rev Cancer.* 2012;12(4):252-264.

6. Postow MA, Callahan MK, Wolchok JD. Immune Checkpoint Blockade in Cancer Therapy. *J Clin Oncol.* 2015;33(17):1974-1982.

7. Ramsay AG, Clear AJ, Fatah R, Gribben JG. Multiple inhibitory ligands induce impaired T-cell immunologic synapse function in chronic lymphocytic leukemia that can be blocked with lenalidomide: establishing a reversible immune evasion mechanism in human cancer. *Blood.* 2012;120(7):1412-1421.

8. McClanahan F, Riches JC, Miller S, et al. Mechanisms of PD-L1/PD-1-mediated CD8 T-cell dysfunction in the context of aging-related immune defects in the Eμ-TCL1 CLL mouse model. *Blood.* 2015;126(2):212-221.

9. McClanahan F, Hanna B, Miller S, et al. PD-L1 checkpoint blockade prevents immune dysfunction and leukemia development in a mouse model of chronic lymphocytic leukemia. *Blood.* 2015;126(2):203-211.

10. Cheng G, Yuan X, Tsai MS, Podack ER, Yu A, Malek TR. IL-2 receptor signaling is essential for the development of Klrg1+ terminally differentiated T regulatory cells. *J Immunol.* 2012;189(4):1780-1791.

11. Cibrián D, Sánchez-Madrid F. CD69: from activation marker to metabolic gatekeeper. *Eur J Immunol.* 2017;47(6):946-953.

12. Zelenay S, Lopes-Carvalho T, Caramalho I, Moraes-Fontes MF, Rebelo M, Demengeot J. Foxp3+ CD25- CD4 T cells constitute a reservoir of committed regulatory cells that regain CD25 expression upon homeostatic expansion. *Proc Natl Acad Sci USA.* 2005;102(11): 4091-4096.

13. Okamura T, Sumitomo S, Morita K, et al. TGF-β3-expressing CD4+CD25(-)LAG3+ regulatory T cells control humoral immune responses. *Nat Commun.* 2015;6(1):6329.

14. Asano T, Meguri Y, Yoshioka T, et al. PD-1 modulates regulatory T-cell homeostasis during low-dose interleukin-2 therapy. *Blood.* 2017;129(15): 2186-2197.

15. Wing K, Onishi Y, Prieto-Martin P, et al. CTLA-4 control over Foxp3+ regulatory T cell function. *Science.* 2008;322(5899):271-275.

16. Kronin V, Fitzmaurice CJ, Caminschi I, Shortman K, Jackson DC, Brown LE. Differential effect of CD8(+) and CD8(-) dendritic cells in the stimulation of secondary CD4(+) T cells. *Int Immunol.* 2001;13(4):465-473.

17. Yamazaki S, Dudziak D, Heidkamp GF, et al. CD8+ CD205+ splenic dendritic cells are specialized to induce Foxp3+ regulatory T cells. *J Immunol.* 2008;181(10):6923-6933.

18. Hanna BS, McClanahan F, Yazdanparast H, et al. Depletion of CLL-associated patrolling monocytes and macrophages controls disease development and repairs immune dysfunction in vivo. *Leukemia.* 2016; 30(3):570-579.

19. Elias CG III, Spellberg JP, Karan-Tamir B, et al. Ligation of CD31/PECAM-1 modulates the function of lymphocytes, monocytes and neutrophils. *Eur J Immunol.* 1998;28(6):1948-1958.

TO THE EDITOR:

No red blood cell damage and no hemolysis in G6PD-deficient subjects after ingestion of low vicine/convicine *Vicia faba* seeds

Valentina Gallo,[1] Oleksii A. Skorokhod,[1] Luigi Felice Simula,[2] Tiziana Marrocco,[1] Elisa Tambini,[1] Evelin Schwarzer,[1] Pascal Marget,[3] Gérard Duc,[3] and Paolo Arese[1]

[1]Department of Oncology, University of Torino, Torino, Italy; [2]Department of Clinical Chemistry, Ospedale Civile, Alghero, Italy; and [3]Institut National de la Recherche Agronomique, Unité Mixte de Recherche No. 1347-Agroécologie, Institut National Supérieur de Science Agronomique, Dijon, France

Favism, or "favic crisis," is a potentially life-threatening acute hemolysis elicited in carriers of low-activity glucose 6-phosphate dehydrogenase (G6PD) variants by ingestion of raw faba bean (*Vicia faba* L) (FB) seeds.[1,2] In 2 surveys of hemolytic crises because of favism in Sardinia in 948 children aged 2 to 12 years and 610 adults, hemolysis was elicited by raw beans in 94.4% and 97% of all cases, respectively.[3,4] Low-activity G6PD variants are the Mediterranean variant (1% to 5% residual activity)[2,5] predominantly present in Sardinia and common in Mediterranean and Middle East countries and in the Indian subcontinent,[5] and other G6PD variants common in China and the Far East.[6] FBs are rich in proteins, starch, fibers, vitamins, and minerals and are low in fat.[7] FB seeds are uniquely rich (5-14 g/kg wet weight) with the β-glucosides vicine (V) and convicine (C),[7,8] which generate the redox-active aglycones divicine (D; 2,6-diamino-4,5-dihydroxypyrimidine) and isouramil (I; 6-amino-2,4,5-trihydroxypyrimidine)[1,9] upon hydrolysis by the β-glucosidase very active in raw FBs.[10,11] D/I share an identical mechanism of action and are considered to be causative elements of favism.[9-11] In isolated, oxygenated red blood cells (RBCs), D/I generate semiquinoid free radicals[12] that produce oxygen radicals and hydrogen peroxide,[13] which rapidly oxidize reduced NAD phosphate (NADPH), reduced glutathione (GSH), thiol groups, and membrane lipids of RBCs[10,11,14]; transform oxy-hemoglobin in ferrylhemoglobin, methemoglobin, and hemichromes[11,15-17]; and release iron from hemoglobin and ferritin.[14] Although in D/I-treated G6PD-normal RBCs GSH and NADPH are rapidly regenerated and oxidative modifications reversed, no reversal occurs in D/I-treated G6PD-deficient RBCs.[10,11] Without the protective action of GSH and NADPH, a chain of oxidative events may enhance phagocytic removal of damaged RBCs.[10,11] Indeed, RBCs isolated during hemolytic crisis have shown early decrease of GSH and NADPH[10,11]; peroxidation